Journal of Medicinal Chemistry

Article

pubs.acs.org/jmc

# Modulation of the Fibrillogenesis Inhibition Properties of Two Transthyretin Ligands by Halogenation

Ellen Y. Cotrina,[†] Marta Pinto,[∥,‡] Lluís Bosch,[§] Marta Vilà,[†] Daniel Blasi,[⊥] Jordi Quintana,[⊥] Nuria B. Centeno,[‡] Gemma Arsequell,[§] Antoni Planas,[†] and Gregorio Valencia*[,§]

[†]Laboratory of Biochemistry, Bioengineering Department, Institut Químic de Sarrià, Universitat Ramon Llull, [‡]Pharmacoinformatics Group, Research Programme on Biomedical Informatics (GRIB), Department of Experimental and Health Sciences, Universitat Pompeu Fabra, IMIM (Hospital del Mar Medical Research Institute)-Universitat Pompeu Fabra, [§]Institut de Química Avançada de Catalunya (IQAC−CSIC), [⊥]Drug Discovery Platform, Parc Científic de Barcelona, Barcelona, Spain

Supporting Information

**ABSTRACT:** The amyloidogenic protein transthyretin (TTR) is thought to aggregate into amyloid fibrils by tetramer dissociation which can be inhibited by a number of small molecule compounds. Our analysis of a series of crystallographic protein-inhibitor complexes has shown no clear correlation between the observed molecular interactions and the in vitro activity of the inhibitors. From this analysis, it emerged that halogen bonding (XB) could be mediating some key interactions. Analysis of the halogenated derivatives of two well-known TTR inhibitors has shown that while flufenamic acid affinity for TTR was unchanged by halogenation, diflunisal gradually improves binding up to 1 order of magnitude after iodination through interactions that can be interpreted as a suboptimal XB (carbonyl Thr106: I...O distance 3.96−4.05 Å; C—I...O angle 152−156°) or as rather optimized van der Waals contacts or as a mixture of both. These results illustrate the potential of halogenation strategies in designing and optimizing TTR fibrillogenesis inhibitors.

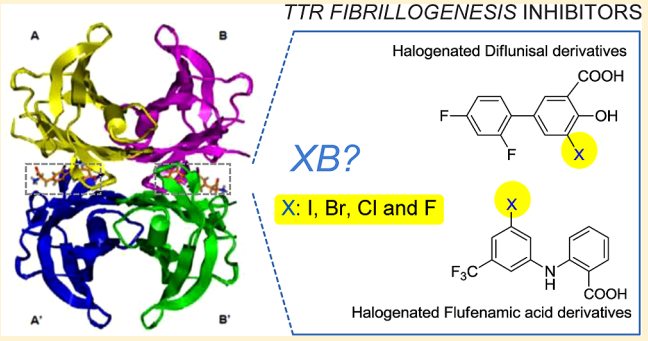


## INTRODUCTION

Mutations in the plasma protein transthyretin (TTR) are the cause of a series of rare but serious amyloid diseases.[1−5] Numerous studies have focused on showing that protein stabilization by low molecular weight compounds can be an effective therapeutic alternative for the TTR-related amyloid diseases,[6−11] which include familial amyloid polyneuropathy (FAP), familial amyloid cardiomyopathy (FAC), senile systemic amyloidosis (SSA), and central nervous system selective amyloidoses (CNSA).[12,13] This concept comes from the observation that thyroxine (T4), the endogenous ligand of transthyretin, is able to inhibit TTR aggregation by stabilizing the tetrameric structure of the protein.[4,14−18] Many different families of compounds are known to stabilize TTR effectively, preventing its aggregation in vitro.[19−24] Within this family of compounds, only a benzoxazole derivative (Tafamidis)[25−28]has reached approval for clinical use in Europe, while a few others (diflunisal, doxycycline/TUDCA) are still under clinical testing.[29−34]Other potential therapeutic strategies are also being explored but are less developed, including immunotherapy,[35,36] gene therapy with small interfering RNAs, antisense oligonucleotides, and single-stranded oligonucleotides.[37−39]

TTR is a 55 kDa homotetrameric protein containing 127 residues per monomer that are organized in eight $\beta$ strands, named from A to H and connected by loops and a short $\alpha$ helix between E and F strands (Figure 1).[40−43] The association of two monomers (A and B) leads to a dimer (AB), and the two dimers (AB and A′B′) assemble to form the functional tetramer that features a central channel at the dimer−dimer interface where the two chemically equivalent hormone binding sites, named A-A′ and B-B′, respectively, are located (Figure 1).

A relevant feature of the TTR binding sites is the presence of three symmetry-related depressions termed halogen binding pockets (HBPs),[16] which accommodate the iodine atoms of the thyroid hormones in their complexes with TTR.[44] The innermost pockets are HBP3 and HBP3′, and the outermost are HBP1 and HBP1′ (Figure 2).

Structural information on TTR is extensive as exemplified by the nearly 200 TTR-related entries[45] that are currently collected at the Protein Data Bank (http://www.rcsb.org).[46]With the aim to devise new strategies for the design of more effective TTR tetramer stabilizing ligands, we have sampled and computationally analyzed this PDB information on TTR. Attention has been paid to the in silico study of ligand−HBPs interactions and to experimentally evaluate the effects of introducing homologous series of halogen atoms into

**Received:** July 15, 2013
**Published:** October 23, 2013

  

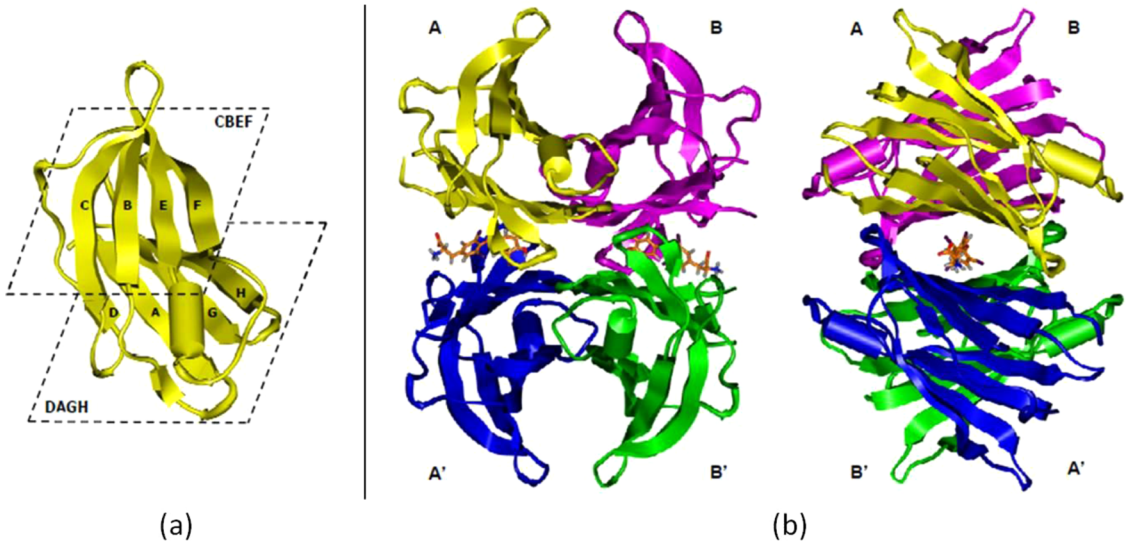


**Figure 1.** (a) $\beta$-Sheet topology of each TTR monomer. (b) Tetrameric structure of TTR (two views at 90° rotation on the $y$-axis) showing the two symmetric T4 binding sites.

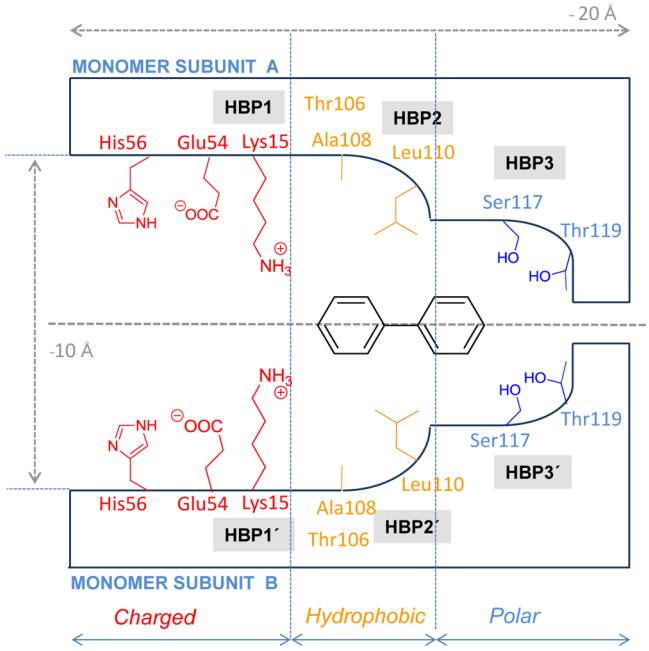


**Figure 2.** Schematic representation of the three chemical regions in which TTR binding sites can be divided, showing also the halogen binding pockets (HBPs) location.

ligands to see if new sites of molecular recognition mediated by halogen bonding could be created.[47−55]

## RESULTS AND DISCUSSION

**Ligand Selection.** The most noticeable feature of the TTR crystallographic complexes deposited at the Protein Data Bank is the wide diversity of chemical structures (more than 40 different scaffolds) that binds TTR. From these diverse structures, we selected 13 (Figure 3), including the endogenous ligand of TTR, thyroxine (**1**) and a close derivative (**2**), therapeutic drugs such as flurbiprofen (**3**), flufenamic acid (**4**), and diclofenac (**5**), natural products like retinoic acid (**6**) and resveratrol (**7**), and six synthetic compounds (**8**−**13**), one of which is iododiflunisal (**13**), a drug candidate developed by us.[56]

**In Vitro Inhibition Activity.** To obtain homogeneous inhibition data to conduct the SAR studies of interest, all of these 13 compounds were tested in a turbidimetric in vitro assay to evaluate their potential activity as TTR fibril inhibitors.[57,58] The protocol uses a highly amyloidogenic TTR variant (Y78F) which enables kinetic monitoring of protein aggregation in short time under acid-induced fibrillogenesis conditions. One of the parameters that can be assessed by this method is the $IC_{50}$ value, which is the concentration of inhibitor at which the initial rate of fibril formation is half than in the absence of inhibitor. A second parameter is the percentage of reduction in fibril formation rate (RA%) at a high concentration of test compound relative to the rate obtained in the absence of the compound. RA values of 100% indicate that the inhibitor is able to fully prevent the formation of fibrils. Both values are reported in Table 1, which shows that the polychlorinated biphenyl **9** followed by **13**, **7**, **2**, **4**, and **6** are the best inhibitors. Conversely, **3** and **5** exhibited the poorest activity.

**Structural Analysis of TTR−Ligand Interactions.** After processing the 3D structure of these 13 TTR crystallographic complexes (see Supporting Information Comment 1), one of the first observations was that the amino acid side chains protruding into the two chemically equivalent binding sites of TTR show great flexibility. Thus, we have found different residues that are able to adopt various rotameric conformations within the same crystal structure. This is the case of the TTR−(**5**) complex, where two different conformers for residues Leu17, Ser117, and Thr119 exist. We have also found evidence for ligand-dependent conformational arrangements upon binding for the side chains of Lys15, Glu54, Thr106, Ser115, Ser117, and Thr119. Among them, Lys 15 is the residue which exhibits the highest conformational variability, which is driven to maximize in each case hydrophobic interactions between the methylene groups of the lysine and the aromatic or hydrophobic moieties of the ligand placed at the entry of the cavity. Furthermore, it allows the formation of hydrogen bonds between the $\varepsilon$-NH2 and any other hydrophilic group on the ligand (see Supporting Information Comment 2).


dx.doi.org/10.1021/jm401061w | J. Med. Chem. 2013, 56, 9110−9121

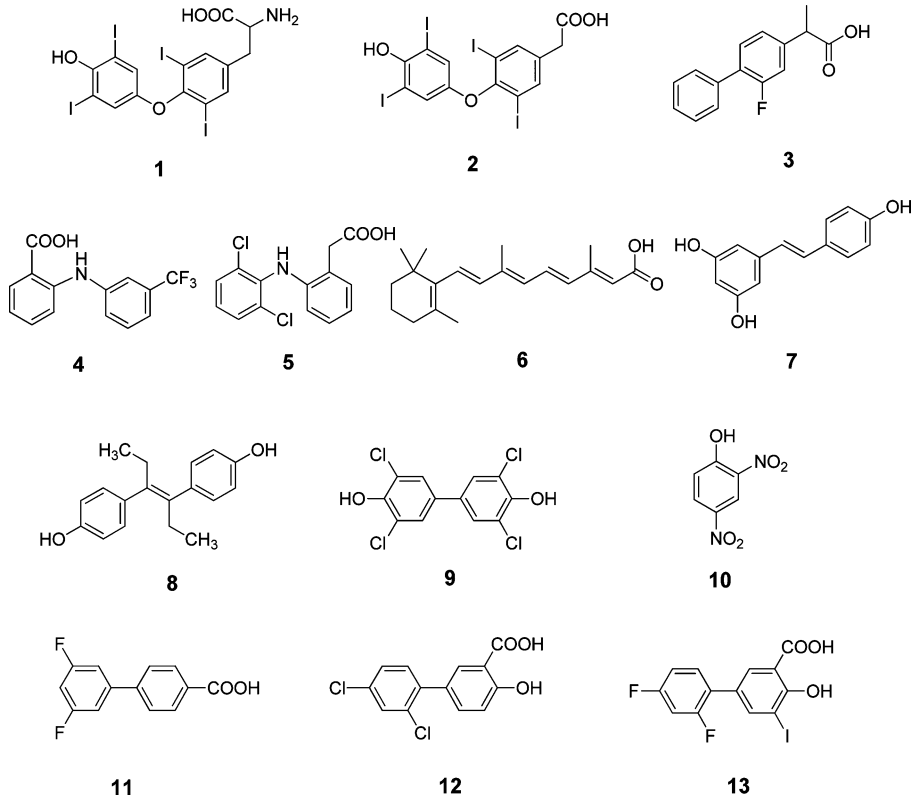


**Figure 3.** Selected ligands from TTR–ligand complexes available at the PDB: (**1**) thyroxine or T4; ( **2**) 3,3′,5,5′-tetraiodothyroacetic acid or T4Ac; (**3**) flurbiprofen; (**4**) flufenamic acid; (**5**) diclofenac; (**6**) retinoic acid; (**7**) resveratrol; (**8**) diethylstilbestrol; (**9**) 3,5,3′,5′-tetrachlorobiphenyl-4,4′-diol; (**10**) 2,4-dinitrophenol; (**11**) 3′,5′-difluorobiphenyl-4-carboxylic acid; (**12**) 2′,4′-dichloro-4-hydroxy-1,1′-biphenyl-3-carboxylic acid, and (**13**) iododiflunisal. (See Figure S0 in Supporting Information for more details on the related PDB structures.)

**Table 1. Inhibition of Acid-Induced Fibrillogenesis by Ligands (IC50 and RA%) Measured by the Kinetic Turbidimetric Assay and Structural Properties of the TTR–Ligand Crystallographic Complexes**[a]

| | fibrillogenesis inhibition | | X-ray features of TTR–ligand complexes | | | | | | | |
|---|---|---|---|---|---|---|---|---|---|---|
| | | | | | occupation of HBP pockets by the ligands | | | | | |
| ligand | $IC_{50}$ ($\mu$M) | RA (%) | PDB | binding mode | HBP1 | HBP1′ | HBP2 | HBP2′ | HBP3 | HBP3′ |
| **1** | 10.5 | 80 | 2ROX | F | –I | –I | | –I | –I | |
| **2** | 4.8 | 93 | 1Z7J | F | –I | –I | | –I | –I | |
| | | | | R | –I | –I | | –I | –I | –CH– |
| **3** | >100 | 35 | 1DVT | R | | | | –F | –CH– | –CH– |
| **4** | 6.2 | 89 | 1BM7 | F | | | | | | $-CF_3$ |
| **5** | 26 | 74 | 1DVX | R | | –CH– | | | –CH– | –COOH |
| **6** | 8.1 | 100 | 1TYR | F | $-CH_2-$ | | | | $-CH_3$ | $-CH_3$ |
| **7** | 4.5 | 89 | 1DVS | F | –OH | –OH | | | –CH– | –CH– |
| **8** | 16.6 | 67 | 1TT6 | F | –CH– | –CH– | $-CH_2-CH_3$ | $-CH_2-CH_3$ | –CH– | –CH– |
| **9** | 2.1 | 100 | 2G5U | R | –Cl | –Cl | | | –Cl | –Cl |
| **10** | 20 | 77 | 2B15 | R | | | | | $-NO_2$ | –CH– |
| **11** | 10.8 | 89 | 2B9A | R | | | | | –CH– | –CH– |
| **12** | 12.8 | 75 | 2B77 | R | | | | | –CH– | –COOH |
| **13** | 4.5 | 94 | 1Y1D | F | –OH | | –I | | –F | –F |

[a]See Supporting Information Comment 1 for more details on the PDB structures.

Upon ligand binding, other important conformational and structural rearrangements suffered by TTR also involve the side chains of Ser117 and Thr119 (see Supporting Information Comment 3), modifying the surface polarity of the HBP3/3′ pockets. Consequently, these pockets are able to accommodate a wide variety of chemical groups (Table 1), varying from hydrophobic (such as compounds **4** or **6**) to negatively charged groups (such as compounds **5** or **12**). The conformation adopted by Ser117 and Thr119 facilitates the binding of the ligands in the so-called forward (F) and reverse (R) binding modes. In the forward mode, the hydrophilic group of the ligand is close to the binding site entrance, favoring electrostatic interactions between the hydrophilic groups located at the entry of the cavity and the residues Lys15 and/or Glu54 of one


dx.doi.org/10.1021/jm401061w | J. Med. Chem. 2013, 56, 9110–9121

or both A and A′ monomers (Table 1). In contrast, other ligands such as **5**, **11**, or **12** bind to TTR in the reverse mode, favoring the formation of a hydrogen bond between the hydrophilic groups positioned near the tetramer center and the residues Ser117 and/or Thr119 of one or both monomers (Table 1). However, no relationship could be found between the binding mode of the studied ligands and their activity (see Table 1 and Supporting Information Comment 4).

One consequence of the discussion above is that ligands are always distributed along the binding sites adopting multiple conformations and even showing different orientations, which makes it very hard to find equivalent functional groups in the same region of the binding site between the studied complexes. This, in turn, precludes the identification of the complementary structural and chemical features on the ligands that may allow formulation of a hypothetic pharmacophoric site on the protein. In addition, the lack of a clear correlation between the ligand structure and its biological activity makes QSAR studies very difficult (Supporting Information Comment 5).

**Role of TTR Halogen Binding Pockets.** A remarkable and unique feature of TTR is the presence of three paired halogen binding pockets (HBPs) on the binding site. Although these pockets were initially described for their ability to accommodate halogen atoms, our modeling analysis has revealed that similar to HBP3 and HBP3′, HBP1/1′ and HBP2/2′ can also accommodate a wide variety of chemical groups due to the conformational flexibility of their constitutive residues (Table 1).

The number of occupied HBPs in the study complexes varies from 2 to 4 with the exception of (**2**) bound in reverse mode and (**8**), which have 5 and 6, respectively. However, there is no relationship between the number of HBP pockets occupied by the ligand and its activity, although the most active compounds are characterized by the presence of a halogen atom in the HBP1/1′ and/or HBP3/3′ (Table 1).

**Experimental Examination for Halogen Bonding Interactions.** Halogen bonding interactions (XB)[59] are widespread in biological systems,[60] but only recently they have raised considerable interest in medicinal chemistry.[47−55] Of particular interest to the present work are the attempts to use XB as a design feature to stabilize protein structures.[61,62] This type of interaction occurs when a halogen forms direct close contacts of the type R−X···Y, where the halogen X acts as a Lewis acid and Y can be any kind of electron donor (Lewis base).[63,64] It is driven by the $\sigma$-hole, a positively charged region on the hind side of X along the R−X bond axis caused by anisotropy of electron density on the halogen.[51] The possibility that XB formation may play a role in stabilizing TTR−ligand tetrameric complexes has been previously examined in the literature by analyzing the crystallographic complexes between TTR and halogenated ligands: 3,5-diiodosalicylic acid (PDB entry 3B56),[65] two brominated stilbenes (PDB entries 3IMU and 3IMV),[66] and diclofenac (PDB entry 1DVX).[6] It was found that one iodine atom of the diiodosalicylic acid binds to the backbone carbonyl group of Ser117 [I(1)...O distance: 3.50 Å; C−I(1)...O angle: 148.3°]. Similarly, the bromine atoms of the stilbenes bind to the same Ser117 carbonyl [Br...O distances: 3.33 and 3.39 Å; C−Br...O angles: 145.9 and 143.5°]. In the case of diclofenac, there is also the possibility that the Cl(4) atom may interact with the hydroxyl oxygen atom of Thr119 forming an XB.[47] Also, the crystal structure of the piscine TTR complex with thyroxine (PDB-ID: 1SN0)[67] has been examined for XB. Thyroxine (**1**) binds to TTR, forming two equivalent XBs with two neighboring subunits. Both interaction geometries between the iodine atoms and the backbone carbonyls of Leu109 residues (equivalent to human Ala 109) are close to optimal [I...O distances: 3.29 and 3.35 Å; $\sigma$-hole angles: 162.3 and 169.7°]. These XBs are also orthogonal with hydrogen bonds between the backbone carbonyls of the same Leu109 and the backbone amide NH of Leu17 [$\alpha$X...O...H(N) angles of 88 and 90°].[51]

Here, we are further addressing experimentally the halogen bonding issue on TTR−ligand complex formation with the aim to propose and evaluate a predictive modeling approach for the optimization of TTR ligand affinity by XB formation. Thus, we have carried out the synthesis and biochemical study of two homologous series of halogenated derivatives of flufenamic acid and diflunisal, two NSAIDs which are well-known TTR ligands.[68,69]

From previous studies,[70] we have experimental evidence that iodination at the C-4 position of flufenamic acid completely abolishes the TTR fibrillogenesis inhibition of the parent compound **4**. Similarly, addition of an iodine atom at position 4′ of flurbiprofen (compound **3**) did not improve its potency. However, iodination of diflunisal at the 5 position (see below) significantly increased the potency of this compound. Taken together, these results suggested that the incorporation of an iodine (halogen) atom does not always improve the potency of a compound. In other words, not any position of the ligand seems favorable for halogenation.

In this scenario, in order to explore in a predictive fashion the use of halogen bonding interactions for the optimization of the fibrillogenesis inhibition potency of this ligand, the most energetically favored halogenation position that induces the best fit of the halogen on the HBPs was calculated. As discussed above, it was assumed that HBPs are the most suitable places evolved by nature on TTR to interact with halogen atoms. Accordingly, the GRID software[71] was used to predict which positions of flufenamic acid are the most favorable for halogenation. From these contour maps, it was shown that the most energetically favored position of (**4**) for halogenation is the C-5′ position, and that the interaction energy of the halogen located at this position and the protein decreases from iodine to fluorine. Interestingly, all these ligands are characterized by presenting the 3′- and 5′-halogenated groups into the HBP3 and HBP3′ pockets, respectively.

The homologous series of halogenated derivatives at C-5′ (**18**−**21**) (Figure 4) was synthesized and, along with the parent

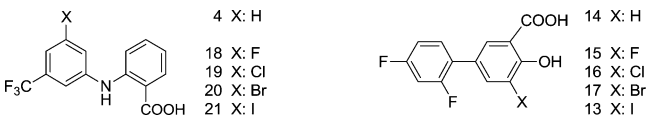


**Figure 4.** Halogenated flufenamic acid (**18**−**21**) and diflunisal (**15**−**17** and **13**) analogues in this study.

compound (**4**), the compounds were tested in the kinetic turbidity assay described above (see Chemistry section in Supporting Information). Their fibrillogenesis inhibition properties expressed by the parameters $IC_{50}$ and RA (%) are reported in Table 2. Moreover, binding of the ligands to the Y78F-TTR variant was determined by isothermal titration calorimetry (ITC), which provides the thermodynamic parameters $K_d$, $\Delta H$, and $T\Delta S$ of binding under conditions where no protein aggregation occurs (pH = 7). Although the


dx.doi.org/10.1021/jm401061w | J. Med. Chem. 2013, 56, 9110−9121

**Table 2. Inhibition of Acid-Induced TTR Fibrillogenesis (Turbidity Assay) and Ligand Binding (Isothermal Titration Calorimetry) of Halogenated Flufenamic Acid and Diflunisal Derivatives to TTR Y78F Variant[a]**

| | | inhibition (turbidity assay) | | binding (isothermal titration calorimetry) | | | |
|---|---|---|---|---|---|---|---|
| No. | X | $IC_{50}$ ($\mu$M) | RA (%) | $K_d$ (nM) | $\Delta H$ (kcal/mol) | $T\Delta S$ (kcal/mol) | $\Delta G$ (kcal/mol) |
| flufenamic acid derivatives | | | | | | | |
| **4** | H | 6.2 | 89 | 109 | −10.7 | −1.2 | −9.5 |
| **18** | F | 6.5 | 91 | 91 | −17.7 | −8.1 | −9.6 |
| **19** | Cl | 6.0 | 86 | 86 | −14.8 | −4.0 | −10.8 |
| **20** | Br | 5.9 | 91 | 64 | −12.9 | −3.1 | −9.8 |
| **21** | I | 6.4 | 94 | 85 | −10.1 | −0.47 | −9.6 |
| diflunisal derivatives | | | | | | | |
| **14** | H | 18 | 85 | 1160 | −8.16 | −0.05 | −8.1 |
| **15** | F | 7.6 | 87 | 1120 | −8.45 | −0.32 | −8.1 |
| **16** | Cl | 7.5 | 89 | 375 | −5.93 | 2.8 | −8.8 |
| **17** | Br | 5.6 | 88 | 194 | −8.65 | 0.51 | −9.2 |
| **13** | I | 4.5 | 94 | 87 | −7.52 | 2.1 | −9.66 |

[a]Turbidity assay: 0.4 mg/mL TTR-Y78F, 0−40 $\mu$M inhibitor, pH 4.2, 37 °C. Isothermal titration calorimetry: 20−30 $\mu$M TTR-Y78F, 0−120 $\mu$M ligand, pH 7.6, 25 °C.

two symmetrical binding sites of TTR show negative cooperativity for T4 binding,[72,73] a simple binding model with two identical sites gave the best fitting of the calorimetric data (Table 2).

As seen in Table 2, flufenamic acid (**4**) is a good TTR fibrillogenesis inhibitor for which halogenation at C-5′ does not significantly increase the inhibition potency of the parental compound. Likewise, the ligand binding affinity data ($K_d$) of the compounds between 100 and 60 nM loosely correlate with the van der Waals radii of the halogen atoms and with the increasing affinity predicted by the GRID calculations, suggesting that no stabilizing halogen bonding interactions seem to be at play in this series of halogenated compounds.

On the other hand, previous studies[74−76] have experimentally evidenced that iodination at the 5 position of diflunisal led to a much efficient TTR fibrillogenesis inhibitor, namely, iododiflunisal (**13**) (Table 1). To seek if this enhanced potency could be caused by an XB that arises by the presence of the iodine atom, we have synthesized the three remaining compounds of the homologous series of halogen-substituted diflunisal derivatives having F, Cl, and Br at the 5 position. The synthesis of the series (**15**, **16**, **17**) was effected by conventional aromatic electrophilic halogenation methods (Figure 4 and Supporting Information Chemistry section).

The whole series of halogenated diflunisal derivatives and the parent compound (**13**−**17**) were tested for inhibitory activity and affinity toward Y78F-TTR (Table 2). The inhibition values of this series clearly indicate that the introduction of a halogen atom at C-5 of diflunisal always improves its potency. This improvement almost reaches the lowest measurable values of $IC_{50}$ because the assay is run at 7.2 $\mu$M concentration of TTR, the concentration at which the corresponding amount of ligand is required to semisaturate the protein. More interesting is the fact that gradual and large differences in the binding constants ($K_d$) are observed along the series. Such decreases of $K_d$ correlate with increasing halogen volume as measured by their effective van der Waals radii for phenyl substitution[77] (H: 1.20 Å; F: 1.47 Å; Cl: 1.77 Å; Br: 1.92 Å; I: 2.06 Å). The stabilization provided by halogenation reaches more than 1 order of magnitude in terms of the affinity constant for iododiflunisal (**13**), which translates to a gain in free energy of $-\Delta\Delta G = 1.5$ kcal mol$^{-1}$. Indeed, taking also into account the crystallographic information available from the complex of (**13**) and TTR (PDB 1Y1D),[56] these results could be interpreted by a new protein−ligand interaction of XB type arising after the H for X exchange. As shown in Figure 5, in this complex the

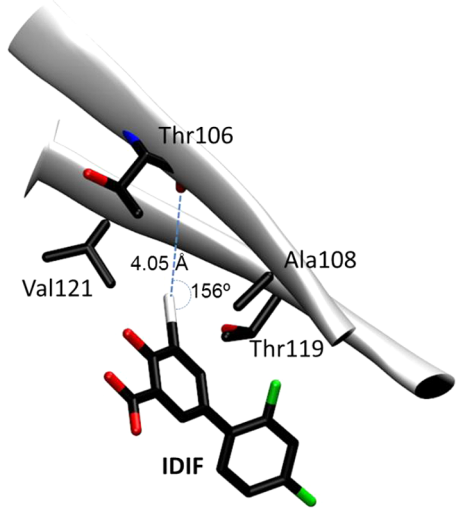


**Figure 5.** TTR−iododiflunisal (**13**) complex. Residues Thr106, Ala108, Thr119, and Val121 shape the halogen binding pocket establishing van der Waals contacts with the iodine atom. Also, a suboptimal XB interaction with the carbonyl group of Thr106 is shown.

iodine atom of (**13**) occupies the HBP1 pocket of TTR through a series of contacts with residues Thr106, Ala108, Thr119, and Val121. The interaction of the iodine with the carbonyl group of Thr106 takes place through a bonding geometry I...O distance of 3.96−4.05 Å and $\sigma$-angle of 152−156° that, following the criteria established by Boeckler,[78] can be regarded as a suboptimal XB. Using the model data provided by these authors, the stabilization energy contributed by this XB may not be more than 50% of the one with an optimal XB geometry I...O distance of 3 Å and $\sigma$-angle of 180°. Nevertheless, other explanations such as optimized van der Waals interactions generated by the increasing volume of the halogen atom in the series which progressively fills the halogen binding pocket and results in better complex stabilization cannot be ruled out. Moreover, the possible effect of an increasing acidity of the phenolic group of (**13**) due to the gradual electron-withdrawing effect of the halogen atoms seems not to be at play (see Figure S7 in Supporting Information).

In summary, both inhibitors, flufenamic acid and diflunisal, show different effects upon halogenation. Flufenamic acid is a good inhibitor with a $K_d$ of 109 nM, and halogenation does not significantly improve binding, meaning that no XB interaction occurs or, if any, its contribution is very small. However, diflunisal is a moderate inhibitor and has a high $K_d$ of 1160 nM, 1 order of magnitude higher than flufenamic acid. In this case, halogenation improves binding significantly through interactions that can be interpreted as suboptimal XB or optimized van der Waals contacts or simultaneous contributions of both,


dx.doi.org/10.1021/jm401061w | J. Med. Chem. 2013, 56, 9110−9121

resulting in an 1 order of magnitude lower $K_d$ (for iododiflunisal), at values similar to those obtained for the flufenamic acid series.

## CONCLUSION

In conclusion, experimental evidence is provided that halogenation of TTR ligands may improve their affinity and fibrillogenesis inhibition properties. In the case of diflunisal, these may take place through new although suboptimal XB interactions and/or by optimized van der Waals contacts. Regardless of their nature, such interactions may serve to optimize the tetramer stabilization properties of TTR ligands. Prediction of the optimal halogenation positions on the ligand is the crucial step and may be guided by directing the desired halogen interactions toward the HBPs of TTR.

## EXPERIMENTAL SECTION

**Chemistry.** TLC analyses were carried out on Merck Kieselgel 60 $F_{254}$ silica gel plates. Visualization was by UV light (254 nm). Chromatographic purification was carried out on silica gel columns 60 (70−200 $\mu$m, 70−230 mesh) from SDS. Solvents for synthesis purposes were used at GPR grade. Reverse-phase HPLC analyses were performed on a Merck-Hitachi (D-6000) HPLC system with an UV L-4000 detector ($\lambda$ = 214 nm), a L-6200 pump, and an AS-2000 automatic injector, using a Merck LiChroCART 250-4 LiChrospher 100-5 RP-C18 column (250 mm × 4.6 mm) with injection volume at 10 $\mu$L and sample concentrations at 1−2 mg/0.5 mL in 50:50 (v/v) acetonitrile/water; the sample was detected at single wavelength of 214 nm with a mobile phase system composed of a mixture of acetonitrile/water, each containing 0.1% of TFA at 1 mL/min flow. The column was maintained at room temperature. The gradient program (GEN1) used was as follows: from an initial (50:50) mixture of A/B to a (10:90) mixture of A/B in 25 min, then back to (50:50) in 15 min. All compounds reported here exhibited spectral data consistent with their proposed structures and had HPLC purities in excess of 95%. Chemical names were generated using ChemBioDraw version by CambridgeSoft. $^1$H and $^{13}$C NMR spectra were recorded at 400 MHz and 100.62 MHz, respectively, in $CDCl_3$ or $(CD_3)_2SO$ on a Varian Mercury-400 spectrometer. Chemical shifts are reported in parts per million (ppm) relative to the residual signal of the deuterated solvent ($\delta$ 7.27 for $^1$H; $\delta$ 77.23 for $^{13}$C) or deuterated or $^{13}$C labeled dimethyl sulfoxide ($\delta$ 2.50 for $^1$H, $\delta$ 39.53 for $^{13}$C) as internal standards. $^1$H NMR data are tabulated in the following order: multiplicity as follows (s, singlet; d, doublet; t, triplet; m, multiplet; br, broad), coupling constants ($J$) are reported in Hertz (Hz), and the number of protons. HRMS spectra (UPLC-TOF/MS) were recorded on a Waters ACQUITY UPLC System with a Waters LCT Premier XE mass spectrometer operating either in the positive ion electrospray mode or in negative electrospray mode. Water and acetonitrile were used as carrier solvents.

**Compound Characterization.** All compounds were obtained in milligram quantities. Details of the synthesis and characterization of each compounds is described below. Selected spectra are included in the Supporting Information. Structures of all reported compounds were confirmed by $^1$H and $^{13}$C NMR and their mass confirmed by HRMS. Purity was determined by HPLC analysis. All reported compounds had >95% purity.

**General Procedure A: Pd(0)-Catalyzed Reaction between 3-Halo-5-(trifluoromethyl)anilines and Methyl 2-bromobenzoate.** A round-bottom flask was charged with $Cs_2CO_3$ (1.20 mmol), *rac*-BINAP (0.05 mmol), and $Pd_2(dba)_3$ (0.025 mmol). The mixture was gently purged with argon, suspended in anhydrous toluene (8 mL), and refluxed for 5 min. Then, a solution of 3-halo-5-(trifluoromethyl)aniline (1.00 mmol) and methyl 2-bromobenzoate (1.10 mmol) in anhydrous toluene (2 mL) was added dropwise. The reaction mixture was refluxed overnight and then diluted with 50 mL of ethyl acetate, filtered over Celite, and evaporated to dryness. The residue was then purified by silica gel column chromatography (hexane/ethyl acetate 85:15).

**General Procedure B: Saponification of Methyl Esters.** To a stirred solution of the corresponding anthranilic methyl ester (1.00 mmol) in 1,4-dioxane (5 mL), was added a solution of LiOH (5.00 mmol) in water (1 mL). The mixture was then heated at 80 °C for 4 h, acidified with 0.25 M HCl (20 mL), and diluted with ethyl acetate (50 mL). The phases were separated, and the aqueous phase was back extracted with more ethyl acetate (25 mL). The organic layer was separated and washed with brine, dried over anhydrous $Na_2SO_4$, and concentrated. The residue was purified by silica gel column chromatography (hexane/ethyl acetate 1:1) to afford the pure acid.

**Methyl *N*-(3-fluoro-5-(trifluoromethyl)phenyl)-anthranilate (18a) General Procedure A.** The title compound was produced from 3-fluoro-5-(trifluoromethyl)-aniline (361 mg, 2.01 mmol) and methyl 2-bromobenzoate (337 $\mu$L, 2.4 mmol). Silica gel column chromatography afforded **18a** (534 mg, 85%) as a white solid. RP-HPLC-(GEN1): RT = 23.85 min. $^1$H NMR (500 MHz, $CD_3COCD_3$): 3.91 (s, 3H), 6.98 (ddd, $J$ = 16.5, 11.0, 3.5, 1H), 7.04−7.12 (m, 1H), 7.34 (dt, $J$ = 18.0, 3.5, 1H), 7.41 (m, 1H), 7.45−7.47 (m, 2H), 8.00 (ddd, $J$ = 13.5, 2.5, 1.1, 1H), 9.63 (br s, 1H). $^{13}$C NMR (75 MHz, $CD_3COCD_3$): 53.3, 107.1 (dq, $J$ = 25.1, 3.5), 111.1 (d, $J$ = 24.8), 114.0 (dq, $J$ = 3.3, 3.3), 116.5, 117.7, 121.6, 125.1 (qd, $J$ = 267.4, 5.2), 133.4, 133.8 (qd, $J$ = 34.2, 12.3), 136.0, 146.5 (d, $J$ = 10.7), 146.5, 165.1 (d, $J$ = 244.5), 169.8. HRMS (ESI$^+$): calcd for $[C_{15}H_{11}F_4NO_2 + H]^+$, 314.0799; found, 314.0806.

***N*-(3-Fluoro-5-(trifluoromethyl)phenyl)anthranilic acid (18).** The title compound was produced by general procedure B from **18a** (200 mg, 0.64 mmol). Silica gel column chromatography afforded **18** (190 mg, 89%) as a white solid. RP-HPLC (GEN1): RT = 14.93 min. $^1$H NMR (500 MHz, DMSO-$d_6$): 6.99 (ddd, $J$ = 9.0, 7.0, 1.0, 1H), 7.13 (dt, $J$ = 8.5, 1.5, 1H), 7.30−7.38 (m, 2H), 7.40 (dd, $J$ = 8.0, 1.0, 1H), 7.50 (ddd, $J$ = 10.0, 6.5, 1.5,1H), 7.94 (dd, $J$ = 8.0, 2.0, 1H), 9.65 (s, 1H). $^{13}$C NMR (100 MHz, $CDCl_3$): 104.8 (dq, $J$ = 25.5, 3.8), 108.8 (d, $J$ = 24.7), 111.4, 116.3, 116.7, 120.2, 123.3 (qd, $J$ = 267.1, 3.4), 131.7 (qd, $J$ = 34.2, 12.9), 131.8, 134.0, 143.9, 144.8, (d, $J$ = 11.1), 162.8 (d, $J$ = 243.4), 169.1. HRMS (ESI$^-$): calcd for $[C_{14}H_9F_4NO_2 - H]^-$, 298.0497; found, 298.0482.

**Methyl *N*-(3-chloro-5-(trifluoromethyl)phenyl)-anthranilate (19a) General Procedure A.** The title compound was produced from 3-chloro-5-(trifluoromethyl)-aniline (215 mg, 1.10 mmol) and methyl 2-bromobenzoate (143 $\mu$L, 1.00 mmol). Silica gel column chromatography afforded **19a** (106 mg, 32%) as an oil. Colorless oil. $R_f$ (hexane/EtOAc 70:30) = 0.65. $^1$H NMR (400 MHz, $CDCl_3$): 3.92 (s, 3H), 6.89 (ddd, $J$ = 8.1, 7.2, 1.2, 1H), 7.24 (s, 1H), 7.31−7.36 (m, 2H), 7.38−7.45 (m, 2H), 8.01 (dd, $J$ = 8.0, 1.6, 1H), 9.65


dx.doi.org/10.1021/jm401061w | J. Med. Chem. 2013, 56, 9110−9121

(br s, 1H). $^{13}$C NMR (100 MHz, $CDCl_3$): 52.1, 113.9, 115.7, 115.7 (quad, $J$ = 3.8), 119.2 (quad, $J$ = 3.9), 119.3, 123.1 (quad, $J$ = 1.0), 123.2 (quad, $J$ = 272.9), 131.9, 133.0 (quad, $J$ = 32.9), 134.3, 135.7, 143.2, 145.5, 168.7. HRMS ($ESI^+$): calcd for $[C_{15}H_{11}ClF_3NO_2 + H]^+$, 330.0504, 332.0527; found, 330.0528, 332.0507.

***N*-(3-Chloro-5-(trifluoromethyl)phenyl)anthranilic acid (19) General Procedure B.** The title compound was produced from **19a** (65 mg, 0.197 mmol). Silica gel column chromatography afforded **19** (41 mg, 66%) as a white solid. RP-HPLC(GEN1): RT = 17.49 min. $R_f$ (hexane/EtOAc 50:50) = 0.16. $^1$H NMR (400 MHz, DMSO-$d_6$): 6.97 (ddd, $J$ = 8.1, 7.2, 1.1, 1H), 7.31 (m, 1H), 7.36 (dd, $J$ = 8.4, 1.1, 1H), 7.45−7.48 (m, 1H), 7.50 (ddd, $J$ = 7.2, 7.0, 1.6, 1H), 7.51−7.53 (m, 1H), 7.92 (dd, $J$ = 7.9, 1.6, 1H), 9.58 (s, 1H), 13.21 (br s, 1H). $^{13}$C NMR (100 MHz, $CDCl_3$): 113.9 (quad, $J$ = 3.7), 116.6, 116.9, 117.4 (quad, $J$ = 4.0), 120.5, 121.6, 123.3 (quad, $J$ = 273.0), 131.5 (quad, $J$ = 32.5), 132.0, 134.2, 134.9, 143.9, 144.4, 169.2. HRMS ($ESI^-$): calcd for $[C_{14}H_9ClF_3NO_2 - H]^-$, 314.0201, 316.0171; found, 314.0220, 316.0161.

**Methyl *N*-(3-bromo-5-(trifluoromethyl)phenyl)-anthranilate (20a) General Procedure A.** The title compound was produced from 3-bromo-5-(trifluoromethyl)-aniline (240 mg, 1.000 mmol) and methyl 2-bromobenzoate (351 μL, 2.50 mmol). Silica gel column chromatography afforded **20a** (106 mg, 32%) as a yellowish wax. RP-HPLC (GEN1): RT = 25.17 min. $R_f$ (hexane/EtOAc 85:15) = 0.40. $^1$H NMR (400 MHz, $CDCl_3$): 3.92 (s, 3H), 6.89 (ddd, $J$ = 8.1, 7.1, 1.2, 1H), 7.32 (dd, $J$ = 8.5, 1.1, 1H), 7.39 (dd, $J$ = 1.8, 0.7, 1H), 7.43 (dddd, $J$ = 8.4, 7.2, 1.7, 0.5, 1H), 7.55 (tt, $J$ = 1.9, 0.5, 1H), 8.01 (ddd, $J$ = 8.0, 1.7, 0.4, 1H), 9.64 (s, 1H). $^{13}$C NMR (100 MHz, $CDCl_3$): 52.1, 113.8, 114.8, 115.8 (quad, $J$ = 3.8), 119.3 (quad, $J$ = 1.0), 121.9 (quad, $J$ = 3.8), 123.2 (quad, $J$ = 272.9), 123.3, 126.0, 133.1 (quad, $J$ = 32.9), 131.9, 134.3, 143.2, 145.5, 168.7. HRMS ($ESI^+$): calcd for $[C_{15}H_{11}BrF_3NO_2 + H]^+$, 373.9999, 375.9978; found, 374.0025, 375.9985.

***N*-(3-Bromo-5-(trifluoromethyl)phenyl)anthranilic acid (20) General Procedure B.** The title compound was produced from **20a** (100 mg, 0.27 mmol). Silica gel column chromatography afforded **20** (83 mg, 86%) as a white solid. RP-HPLC(GEN1): RT = 18.23 min. $R_f$ (hexane/EtOAc 70:30) = 0.15. $^1$H NMR (400 MHz, DMSO-$d_6$): 6.97 (ddd, $J$ = 7.4, 7.3, 1.1, 1H), 7.30 (dd, $J$ = 13.0, 1.1, 1H), 7.39−7.42 (m, 1H), 7.44 (dd, $J$ = 3.6, 1.7, 1H), 7.45−7.48 (m, 1H), 7.60−7.63 (m, 1H), 7.92 (t, $J$ = 2.0, 1H), 9.70 (br s, 1H). $^{13}$C NMR (100 MHz, DMSO-$d_6$): 114.1 (quad, $J$ = 4.3), 116.7, 119.9 (quad, $J$ = 3.8), 120.2, 120.3, 122.9, 123.0 (quad, $J$ = 267.7), 124.4, 131.8 (quad, $J$ = 32.0), 131.9, 133.8, 143.9, 144.4, 169.2. HRMS ($ESI^-$): calcd for $[C_{14}H_9BrF_3NO_2 - H]^-$, 357.9696, 359.9675; found, 357.9671, 359.9658.

**Methyl *N*-(3-(tributylstannyl)-5-(trifluoromethyl)-phenyl)anthranilate (21a).** A round-bottom flask was charged with LiCl (31 mg, 0.720 mmol), $Pd(PPh_3)_4$ (50 mg, 0.043 mmol), and **20a** (54 mg, 0.144 mmol). The flask was purged with argon, and anhydrous 1,4-dioxane (1.5 mL) was added. Then, $(SnBu_3)_2$ (144 μL, 0.288 mmol) was added, and the solution was refluxed for 4 h. The crude reaction mixture was adsorbed on silica gel and purified by silica gel column chromatography (hexane/ethyl acetate 7:3) to afford **21a** (40 mg, 50%) as an oil. Colorless oil. $R_f$ (hexane/EtOAc 70:30) = 0.51. $^1$H NMR (400 MHz, $CDCl_3$): 0.92 (t, $J$ = 7.3, 9H), 1.22−1.42 (m, 12H), 1.59−1.70 (m, 6H), 3.93 (s, 3H), 6.86 (ddd, $J$ = 8.0, 7.0, 1.3, 1H), 7.32−7.44 (m, 2H), 7.46 (s, 1H), 7.53 (s, 1H), 7.57 (s, 1H), 8.01 (dd, $J$ = 8.1, 1.6, 1H), 9.71 (br s, 1H).

**Methyl *N*-(3-iodo-5-(trifluoromethyl)phenyl)-anthranilate (21b).** Compound **21a** (73 mg, 0.126 mmol) was dissolved in acetonitrile, and NaI (21 mg, 0.140 mmol) and *N*-chlorosuccinimide (17 mg, 0.140 mmol) were added. The mixture was stirred for 30 min at rt and diluted with ethyl acetate (20 mL), water (10 mL), and 5% sodium thiosulfate solution (3 mL). Phases were separated, and the aqueous phase was extracted again with ethyl acetate (10 mL). The organic layer was dried over $Na_2SO_4$ anhydrous, filtered, and evaporated to dryness. Purification by silica gel column chromatography (hexane/ethyl acetate (85:15)) afforded **21b** (42 mg, 79%) as an oil. Yellowish wax. $R_f$ (hexane/EtOAc 85:15) = 0.40. $^1$H NMR (400 MHz, $CDCl_3$): 3.92 (s, 3H), 6.88 (ddd, $J$ = 8.2, 7.1, 1.1, 1H), 7.30 (dd, $J$ = 8.5, 1.1, 1H), 7.39−7.45 (m, 2H), 7.58 (s, 1H), 7.75 (s, 1H), 8.02 (dd, $J$ = 8.0, 1.7, 1H), 9.61 (br s, 1H). HRMS ($ESI^+$): calcd for $[C_{15}H_{11}F_3INO_2 + H]^+$, 421.9859; found, 421.9873.

***N*-(3-Iodo-5-(trifluoromethyl)phenyl)anthranilic acid (21) General Procedure B.** The title compound was produced from **21b** (42 mg, 0.100 mmol). Silica gel column chromatography afforded **21** (17 mg, 41%) as a white solid. $R_f$ (hexane/EtOAc 70:30) = 0.15. RP-HPLC (GEN1): RT = 19.27 min. $^1$H NMR (400 MHz, $CDCl_3$): 6.89 (ddd, $J$ = 8.1, 7.1, 1.2, 1H), 7.24−7.27 (m, 1H), 7.35−7.41 (m, 2H), 7.51 (s, 1H), 7.70 (s, 1H), 8.01 (dd, $J$ = 8.0, 1.6, 1H), 9.68 (br s, 1H).: $^1$H NMR (400 MHz, DMSO-$d_6$): 6.98 (dt, $J$ = 7.4, 1.1, 1H), 7.32 (dd, $J$ = 12.9, 1.0, 1H), 7.45−7.48 (m, 1H), 7.48 (dd, $J$ = 3.6, 1.7, 1H), 7.52−7.55 (m, 1H), 7.77−7.80 (m, 1H), 7.94 (t, $J$ = 2.0, 1H), 9.67 (br s, 1H). $^{13}$C NMR (100 MHz, DMSO-$d_6$): 95.9, 114.7 (quad, $J$ = 4.1), 116.4, 120.4, 123.0 (quad, $J$ = 272.9), 125.8 (quad, $J$ = 3.7), 130.6, 131.8 (quad, $J$ = 32.1), 131.9, 134.0, 143.9, 144.0, 169.2. HRMS ($ESI^-$): calcd for $[C_{14}H_9F_3INO_2 - H]^-$, 405.9557; found, 405.9558.

**3-Fluoro-5-iodosalicylic acid (15b).** To a stirred solution of 3-fluorosalicylic acid (**15a**) (158 mg, 1.000 mmol) in $CH_2Cl_2$ (15 mL) was added, in small portions, $IPy_2BF_4$ (409 mg, 1.100 mmol). The mixture was stirred at rt for 2 h and then diluted with ethyl acetate (50 mL), washed with 0.5 M HCl (2 × 10 mL), with brine (15 mL) and dried over anhydrous $Na_2SO_4$, filtered, and evaporated to dryness. The residue was further purified by silica gel column chromatography ($CH_2Cl_2$/MeOH/AcOH (90:10:0.5)) to afford pure **15b** (264 mg, 94%) as a white solid. $R_f$ ($CH_2Cl_2$/MeOH/AcOH 90:10:0.5) = 0.13. $^1$H NMR (400 MHz, DMSO-$d_6$) $\delta$ (ppm): 7.78−7.82 (m, 3H). $^{13}$C NMR (100 MHz, DMSO-$d_6$) $\delta$ (ppm): 78.8 (d, $J$ = 7.0), 118.0 (d, $J$ = 3.4), 129.2 (d, $J$ = 19.7), 133.8 (d, $J$ = 3.7), 149.2 (d, $J$ = 13.0), 151.0 (d, $J$ = 249.3), 169.8 (d, $J$ = 3.4). HRMS ($ESI^-$): calcd for $[C_7H_4FIO_3 - H]^-$, 280.9116; found, 280.9119.

**2′,4′,5-Trifluoro-4-hydroxy-[1,1′-biphenyl]-3-carboxylic acid (15).** Under Ar atmosphere, degassed water (2.5 mL) was added over a mixture of (2,4-difluorophenyl)boronic acid (45 mg, 0.285 mmol), sodium carbonate (82 mg, 0.774 mmol), $Pd(OAc)_2$ (0.6 mg, 1 mol %), and compound **15b** (73 mg, 0.258 mmol). The suspension was stirred at rt for 3 h and then diluted with ethyl acetate (50 mL) and water (10 mL). The pH was adjusted to 2−3 with 0.5 M HCl, and the phases were separated. The aqueous layer was back-extracted with more ethyl acetate (2 × 10 mL), and the combined organic phases were dried over $Na_2SO_4$ anhydrous, filtered, and evaporated to dryness. The residue was purified by silica gel column

chromatography ($CH_2Cl_2$/ethyl acetate/AcOH 50:50:0.5) to afford pure **15** (71 mg, 100%). White solid. $R_f$ ($CH_2Cl_2$/MeOH 85:15) = 0.13. RP-HPLC (GEN1): RT = 10.27 min. $^1$H NMR (400 MHz, DMSO-$d_6$) $\delta$ (ppm): 7.19 (tdd, $J$ = 8.6, 2.6, 1.0, 1H), 7.37 (ddd, $J$ = 11.6, 9.3, 2.6, 1H), 7.62 (td, $J$ = 9.0, 6.5, 1H), 7.70 (ddd, $J$ = 11.9, 2.3, 1.3, 1H), 7.74 (dt, $J$ = 2.5, 1.4, 1H). $^{13}$C NMR (100 MHz, DMSO-$d_6$) $\delta$ (ppm): 104.6 (t, $J$ = 26.0), 112.2 (dd, $J$ = 21.2, 3.8), 115.8 (d, $J$ = 3.9), 121.3 (dd, $J$ = 19.3, 2.4), 122.5−123.1 (m), 124.4 (d, $J$ = 6.7), 125.5 (d, $J$ = 3.0), 131.7 (dd, $J$ = 9.7, 4.4), 149.0 (d, $J$ = 13.1), 150.7 (d, $J$ = 243.6), 159.1 (dd, $J$ = 248.7, 15.5), 161.7 (dd, 260.0, 12.3), 170.9 (d, $J$ = 3.6). HRMS (ESI$^-$): calcd for $[C_{13}H_7F_3O_3 - H]^-$, 268.0347; found, 267.0295.

**5-Chloro-2′,4′-difluoro-4-hydroxy-[1,1′-biphenyl]-3-carboxylic acid (16).** To a stirred solution of diflunisal (50 mg, 0.200 mmol) in acetonitrile (2 mL) was added a solution of *N*-chlorosuccinimide (56 mg, 0.420 mmol) in acetonitrile (1.5 mL). Next, 1 drop of concentrated HCl was added, and the mixture was stirred for 1 h at rt The mixture was then diluted with $CH_2Cl_2$ (20 mL), washed with 5% solution of $Na_2SO_3$ (5 mL) and brine (5 mL), and dried over anhydrous $Na_2SO_4$, filtered, and evaporated to dryness. Further purification by silica gel column chromatography ($CH_2Cl_2$/MeOH/AcOH 95:5:0.5) afforded pure **16** (27 mg, 47%) as a white solid. $R_f$ ($CH_2Cl_2$/MeOH/AcOH 95:5:0.5) = 0.11. RP-HPLC (GEN1): RT = 12.46 min. $^1$H NMR (400 MHz, $CDCl_3$/$CD_3OD$ 95:5) $\delta$ (ppm): 6.86−7.00 (m, 2H), 7.31−7.42 (m, 1H), 7.71 (s, 1H), 7.96 (s, 1H), 9.14 (br s, 1H). $^{13}$C NMR (100 MHz, $CDCl_3$/$CD_3OD$ 95:5) $\delta$ (ppm): 104.5 (dd, $J$ = 25.4, 26.5), 111.7 (dd, $J$ = 21.2, 3.8), 113.9, 122.1, 123.1 (dd, $J$ = 13.6, 4.0), 126.2, 129.3 (d, $J$ = 2.6), 131.0 (dd, $J$ = 9.5, 4.6), 135.9 (d, $J$ = 3.2), 157.0, 159.6 (dd, $J$ = 250.4, 11.9), 162.4 (dd, $J$ = 249.7, 11.8), 178.0. HRMS (ESI$^-$): calcd for $[C_{13}H_7ClF_2O_3 - H]^-$, 282.9979; found, 282.998.

**5-Bromo-2′,4′-difluoro-4-hydroxy-[1,1′-biphenyl]-3-carboxylic acid (17).** To 600 mg of the polymer-bound brominating agent (pyridine hydrobromideperbromide polymer-bound, PVPHP, ∼1 mmol $Br_3$ per g of resin, 3 equiv) in $CH_2Cl_2$ (5 mL), a solution of diflunisal(**14**) (50 mg, 0.200 mmol) in $CH_2Cl_2$ (1 mL) was added and the mixture was shaken o/n. After removing the resin, the filtrate was diluted with more $CH_2Cl_2$ (20 mL), and washed with 5% aq solution of $Na_2SO_3$ (5 mL) and brine (5 mL) and dried over anhydrous $Na_2SO_4$, filtered and evaporated to dryness. Further purification by silica gel column chromatography ($CH_2Cl_2$/MeOH/AcOH 95:5:0.5) afforded pure **17** (34 mg, 52%) as a white solid. RP-HPLC (GEN1): RT = 13.32 min. $^1$H NMR (400 MHz, DMSO-$d_6$) $\delta$ (ppm): 7.17 (ddd, $J$ = 8.5, 8.4, 2.7, 1H), 7.35 (ddd, $J$ = 11.6, 9.3, 2.7, 1H), 7.61 (ddd, $J$ = 9.0, 9.0, 6.6, 1H), 7.92 (t, $J$ = 1.9, 1H), 7.97 (t, $J$ = 1.9, 1H). $^{13}$C NMR (100 MHz, DMSO-$d_6$) $\delta$ (ppm): 104.6 (dd, $J$ = 26.9, 25.9), 110.6, 112.2 (dd, $J$ = 21.1, 3.7), 114.5, 122.6 (dd, $J$ = 13.3, 3.7), 126.1, 129.8 (d, $J$ = 3.5), 131.8 (dd, $J$ = 9.7, 4.4), 138.2 (d, $J$ = 2.3), 157.4, 159.0 (dd, $J$ = 248.4, 11.6), 161.8 (dd, $J$ = 259.7, 11.6), 171.3. HRMS (ESI$^-$): calcd for $[C_{13}H_7BrF_2O_3 - H]$, 326.9473, 328.9453; found, 326.9463, 328.9445.

**2′,4′-Difluoro-4-hydroxy-5-iodo-[1,1′-biphenyl]-3-carboxylic acid or Iododiflunisal (13).** To a solution of 200 mg (0.80 mmol) of diflunisal (**14**) in 5 mL of dichloromethane, 357 mg (1.2 mmol) of $IPy_2BF_4$ was added to obtain a substrate/iodinating reagent ratio of (1:1.5) equiv. The reaction was left under stirring at rt and monitored by HPLC until full conversion to the iodo derivative. After 1.5 h, the solution was diluted with dicloromethane, and the organic phase was successively washed with HCl 1N and a 0.1N sodium thiosulfate solution. The organic phase was dried over $MgSO_4$ and after evaporation yielded a residue (>98% purity), which was further purified by column chromatography on silica gel using $Cl_3CH$/MeOH gradient mixture or HPLC. White solid. HPLC (GEN1): RT = 14.32 min. $^1$H NMR (500 MHz; DMSO-$d_6$) $\delta$ (ppm): 7.12−7.16 (m, 1H). 7.27−7.31 (m, 1H), 7.57 (ddd, $J$ = 9.0, 9.0, 6.5, 1H), 7.92−7.93 (m, 1H), 8.09−8.10 (m, 1H). $^{13}$C NMR (125.7 MHz, DMSO-$d_6$) $\delta$ (ppm): 171.2, 161.6 (dd, $J$ = 12.6, 247.6), 159.7, 158.9 (dd, $J$ = 12.3, 248.5), 144.1, 131.5 (dd, $J$ = 4.5, 9.5), 130.4, 126.8, 122.4 (dd, $J$ = 3.6, 13.3), 113.2, 111.9 (d, $J$ = 20.9), 104.3 (t, $J$ = 26.4), 85.9. HRMS (ESI$^-$): calcd for $[C_{13}H_7F_{2I}O_3 - 1]$, 375,9408; found, 374,9306.

**Protein and Inhibitors.** The human TTR variant Y78F protein was recombinant expressed in *E. coli* and purified as already reported.[57]All assays were performed in buffers containing a final 5% (v/v) DMSO concentration for solubilization of the ligands.

**Kinetic Turbidimetric Assay.** Inhibition of fibrillogenesis was determined by the kinetic turbidimetric assay previously reported.[57,58] Briefly, in seven different wells of a 96-well microplate, 20 $\mu$L of a 4 mg/mL TTRY78F solution in 20 mM potassium phosphate buffer, 100 mM KCl, and 1 mM EDTA at pH 7.6, was mixed with an 80 $\mu$L solution of inhibitor prepared by mixing different volumes of a stock solution of the compound in $H_2O$/DMSO (1:1) to give a range of final compound concentrations of 0−40 $\mu$M. DMSO content was adjusted to a final 5% (v/v), where all ligands tested are soluble. After 30 min incubation at 37 °C with 15 s shaking every minute, 100 $\mu$L of 400 mM KAcO, 100 mM KCl, and 1 mM EDTA buffer at pH 4.2 were added to each well. The final mixture, containing 0.4 mg/mL TTR, 0 to 40 $\mu$M ligand, and 5% DMSO, was incubated at 37 °C with 15 s shaking every minute. Absorbance at 340 nm was monitored for 1.5 h at 1 min intervals. Initial rates of protein aggregation ($v_0$) were obtained from the linear plot absorbance versus time. The dependence of $v_0$ on inhibitor concentration is defined as:

$$v_0 = A + B \cdot \exp^{-C[I]} \quad (1)$$

where $v_0$ is the initial rate of fibril formation (in absorbance units per hour, AU·h$^{-1}$) and [I] the concentration of the inhibitor ($\mu$M).

From the adjustable parameters, the $IC_{50}$ (inhibitor concentration at which the initial rate of protein aggregation is half than that in absence of inhibitor) and RA(%) (percentage reduction of amyloidosis at high inhibitor concentration) were calculated.

**Isothermal Titration Calorimetry Assay.** Dissociation constants for the tested compounds at 25 °C were obtained using a Microcal $iTC_{200}$ isothermal titration microcalorimeter (Microcal, Inc., Northampton, MA). The titrant solution containing 500 $\mu$M compound in 100 mM potassium phosphate, 100 m MKCl, 1 mM EDTA, and 5% (v/v) DMSO at pH 7.6 was placed in the calorimeter syringe. The cell was filled with 20−30 $\mu$M TTR solution (Y78F mutant) prepared in the same previous buffer, filtered through a 0.45 $\mu$m diameter pore membrane, and degassed for 5 min. Protein concentration was determined measuring the absorbance at 280 nm using molar absorptivity of 17 395 M$^{-1}$·cm$^{-1}$ for Y78F monomers, determined by the Bradford assay. An initial 0.5−1


dx.doi.org/10.1021/jm401061w | J. Med. Chem. 2013, 56, 9110−9121

μL initial injection of titrant solution was followed by several 1.5−2 μL injections separated by 150 s. The integration of the thermograms, after subtracting the dilution blanks, gave the binding isotherms that were fitted to a simple binding model with two identical sites by a nonlinear least-squares method using the Origin v.7.0 software provided by Microcal. Dissociation constants were obtained with an 1−5% error.

**Crystallographic Complexes.** Three-dimensional atomic coordinates of the apo-TTR (PDB entry 1BMZ)[79] and the 13 TTR−ligand complexes studied in the present work (PDB entries 1DVT,[6] 2B9A,[68] 2B77,[68] 1Y1D,[56] 2G5U,[80] 1TYR,[81] 2B15,[82] 2ROX,[83] 1Z7J,[84] 1TT6,[85] 1DVS,[6] 1BM7,[79] and 1DVX[6]) were obtained from the structural information available in the Protein Data Bank (PDB).

Before performing the computational analysis of the different TTR−ligand complexes, a previous processing of the PDB files was needed. Considering that the asymmetric crystal unit of all studied complexes is formed by the dimer AB, two ligand molecules (one for each binding site) and water molecules, coordinates for the tetrameric form of TTR were obtained by applying the crystallographic symmetry transformations described in the corresponding PDB file. For residues having multiple conformations, we only considered the one having the highest occupation factor. In the case of having all conformers resolved with the same occupation, we then considered the first one listed in the PDB file. The same procedure was applied for ligands presenting more than one conformation bound to the protein.

**Water Molecule Placement.** Application of the symmetry operations indicated in the corresponding PDB file to obtain the biologically functional tetramer of TTR implies that the distribution of water molecules is exactly the same in both dimers. Owing that this is not the case for nonsymmetric ligands, it was necessary to confirm crystallographic-reported water molecules and propose additional water molecule sites. This strategy allowed us to avoid a symmetrical distribution of water molecules around the ligand, which is an unrealistic description for ligands not possessing 2-fold symmetry.

The GRID v.22a program was applied for water molecule placement in the free and ligand-bound forms of TTR and to validate the ones experimentally determined, as has been previously reported.[71,86−88] To this end, all water molecules present in the crystallographic structures were first removed. The grid box was defined to include the ligand and all the side chains projected into the binding site, yielding a box of dimensions 44 × 40 × 33 Å$^3$. The molecular interaction fields (MIFs) of a standard water probe were calculated into the box using a grid spacing of 0.5 Å. The MINIM program implemented in the GRID package was used to locate the position of the minima in the interaction field, using an energy cutoff of −5 kcal/mol and without interpolation. Finally, these minima were populated with simulated annealing by using the FILMAP utility included in the GRID program package.

**Hydrogen Atoms Refinement.** Added hydrogen atoms were energy minimized by using the parm94 force field implemented in AMBER v.6.[89,90] Ligand partial charges were obtained by computing the electrostatic potentials around the optimized structures at the RH/6-31G* level using Gaussian 94[91] and then fitting the charges by means of the RESP method.[92]

Minimization was carried out using a distance-dependent dielectric constant of 1r to screen for electrostatic interactions and a cutoff distance of 12 Å for van der Waals interactions. Hydrogen atoms refinement was accomplished using 5000 cycles of the steepest descents followed by a conjugate gradient until the maximum gradient of the AMBER energy was smaller than 0.001 kcal/mol Å$^2$.

**Proposal of Halogenated Derivatives.** The GRID v.22a program was also used to propose which positions of flufenamic acid and diflunisal are susceptible to halogenation. To this end, the ligands and water molecules were removed from the crystallographic complexes. The molecular interaction fields (MIF) were generated into the binding site with the GRID halogen probes using the same box dimensions as previously described. Then, superposition of the crystallographic ligands to the corresponding MIFs allowed us to suggest which positions of the ligand are more favorable for halogen substitution.

## ■ ASSOCIATED CONTENT

### Ⓢ Supporting Information

Added comments to the article sections, full description of the synthesis and physicochemical characterization of reported compounds, that is, halogenated flufenamic acids (**18**−**21**) and halogenated diflunisal analogues (**15**−**17** and **13**), and selected spectra (HPLC, $^1$H NMR, $^{13}$C NMR, HRMS) of target compounds. This material is available free of charge via the Internet at http://pubs.acs.org.

## ■ AUTHOR INFORMATION


### Corresponding Author

*E-mail: gregorio.valencia@iqac.csic.es. Ph.: +34934006113

### Present Address

∥Pharmacoinformatics Research Group, Department fur Medizinische, Pharmazeutische Chemie, Universitat Wien, Wien, Austria.


### Author Contributions

Overall research design and writing of the manuscript: J.Q., N.B.C., G.A., A.P., G.V. Chemistry experiments: L.B. Biological experiments: E.Y.C., M.V. Computational studies: M.P., D.B.

### Notes

The authors declare no competing financial interest.

## ■ ACKNOWLEDGMENTS

We thank Dr. Xevi Biarnés for the generation of Figures 5 and S7 and analysis of XB geometries. This work was supported by a Grant No. 080530/31/32 from the Fundació Marató de TV3, Barcelona, Spain.

## ■ ABBREVIATIONS

AcOH, acetic acid; $IPy_2BF_4$, bis(pyridine)iodonium(I) tetrafluoroborate; NCS, *N*-chlorosuccimide; F-TEDA, 1-Chloromethyl-4-fluoro-1,4-diazoniabicyclo[2.2.2]octane bis(tetrafluoroborate); DMSO, dimethylsulfoxide; EtOAc, ethyl acetate; HRMS, high-resolution mass spectrometry; HPLC, high-performance liquid chromatography; $^1$H NMR, proton nuclear magnetic resonance; PVPHP, pyridine hydrobromide perbromide polymer-bound; $Pd(PPh_3)_4$, *Tetrakis*(triphenylphosphine)palladium(0); $(Pd_2(dba)_3)$, *Tris*(dibenzylideneacetone)dipalladium(0); RT, retention time

## ■ REFERENCES

(1) Saraiva, M. J.; Magalhaes, J.; Ferreira, N.; Almeida, M. R. Transthyretin deposition in familial amyloidotic polyneuropathy. *Curr. Med. Chem.* **2012**, *19*, 2304−2311.

(2) Planté-Bordeneuve, V.; Said, G. Familial amyloid polyneuropathy. *Lancet Neurol.* **2011**, *10*, 1086−1097.
(3) Connors, L. H.; Lim, A.; Prokaeva, T.; Roskens, V. A.; Costello, C. E. Tabulation of human transthyretin (TTR) variants. *Amyloid* **2003**, *10*, 160−184.
(4) Saraiva, M. J. Hereditary transthyretin amyloidosis: molecular basis and therapeutical strategies. *Expert Rev. Mol. Med.* **2002**, *4*, 1−11.
(5) Adams, D.; Lozeron, P.; Lacroix, C. Amyloid neuropathies. *Curr. Opin. Neurol.* **2012**, *25*, 564−572.
(6) Klabunde, T.; Petrassi, H. M.; Oza, V. B.; Raman, P.; Kelly, J. W.; Sacchettini, J. C. Rational design of potent human transthyretin amyloid disease inhibitors. *Nat. Struct. Biol.* **2000**, *7*, 312−321.
(7) Johnson, S. M.; Wiseman, R. L.; Sekijima, Y.; Green, N. S.; Adamski-Werner, S. L.; Kelly, J. W. Native state kinetic stabilization as a strategy to ameliorate protein misfolding diseases: a focus on the transthyretin amyloidosis. *Acc. Chem. Res.* **2005**, *38*, 911−921.
(8) Connelly, S.; Choi, S.; Johnson, S. M.; Kelly, J. W.; Wilson, I. A. Structure-based design of kinetic stabilizers that ameliorate the transthyretin amyloidoses. *Curr. Opin. Struct. Biol.* **2010**, *20*, 54−62.
(9) Ando, Y.; Ueda, M. Diagnosis and therapeutic approaches to transthyretin amyloidosis. *Curr. Med. Chem.* **2012**, *19*, 2312−2323.
(10) Sacchettini, J. C.; Kelly, J. W. Therapeutic strategies for human amyloid diseases. *Nat. Rev. Drug Disc.* **2002**, *1*, 267−275.
(11) Ong, D. S.; Kelly, J. W. Chemical and/or biological therapeutic strategies to ameliorate protein misfolding diseases. *Curr. Opin. Cell Biol.* **2011**, *23*, 231−238.
(12) Kapoor, P.; Thenappan, T.; Singh, E.; Kumar, S.; Greipp, P. R. Cardiac amyloidosis: a practical approach to diagnosis and management. *Am. J. Med.* **2011**, *124*, 1006−1015.
(13) Benson, M. D. Amyloidosis. In *The Metabolic Basis of Inherited Disease*, Scriver, C. R., Beaudet, A. L., Sly, W. S., Valle, D., Childs, B., Kinzler, K. W., Vogelstein, B., Eds.; McGraw-Hill: Columbus, OH, 2001; pp 5345−5378.
(14) Saraiva, M. J. Transthyretin amyloidosis: a tale of weak interactions. *FEBS Lett.* **2001**, *498*, 201−203.
(15) Hou, X.; Aguilar, M. I.; Small, D. H. Transthyretin and familial amyloidotic polyneuropathy. Recent progress in understanding the molecular mechanism of neurodegeneration. *FEBS J.* **2007**, *274*, 1637−1650.
(16) de la Paz, P.; Burridge, J. M.; Oatley, S. J.; Blake, C. C. F. Multiple modes of binding of thyroid hormones and other iodothyronines to human plasma transthyretin. In *The Design of Drugs to Macromolecular Targets*; Beddell, C. R. Ed.; John Wiley and Sons: New York, 1992; pp 119−172.
(17) Andrea, T. A.; Cavalieri, R. R.; Goldfine, I. D.; Jorgensen, E. C. Binding of thyroid hormones and analogues to the human plasma protein prealbumin. *Biochemistry* **1980**, *19*, 55−63.
(18) Bartalena, L.; Robbins, J. Thyroid hormone transport proteins. *Clin. Lab. Med.* **1993**, *13*, 583−598.
(19) Almeida, M. R.; Gales, L.; Damas, A. M.; Cardoso, I.; Saraiva, M. J. Small transthyretin (TTR) ligands as possible therapeutic agents in TTR amyloidoses. *Curr. Drug Targets: CNS Neurol. Disord.* **2005**, *4*, 587−596.
(20) Nencetti, S.; Orlandini, E. TTR fibril formation inhibitors: is there a SAR? *Curr. Med. Chem.* **2012**, *19*, 2356−2379.
(21) Alhamadsheh, M. M.; Connelly, S.; Cho, A.; Reixach, N.; Powers, E. T.; Pan, D. W.; Wilson, I. A.; Kelly, J. W.; Graef, I. A. Potent kinetic stabilizers that prevent transthyretin-mediated cardiomyocyte proteotoxicity. *Sci. Transl. Med.* **2011**, *3* (97), 97ra81 DOI: 10.1126/scitranslmed.3002473.
(22) ECGC: Ferreira, N.; Saraiva, M. J.; Almeida, M. R. Natural polyphenols as modulators of TTR amyloidogenesis: in vitro and in vivo evidences towards therapy. *Amyloid* **2012**, *19* (Suppl 1), 39−42.
(23) Kristen, A. V.; Lehrke, S.; Buss, S.; Mereles, D.; Steen, H.; Ehlermann, P.; Hardt, S.; Giannitsis, E.; Schreiner, R.; Haberkorn, U.; Schnabel, P. A.; Linke, R. P.; Röcken, C.; Wanker, E. E.; Dengler, T. J.; Altland, K.; Katus, H. A. Green tea halts progression of cardiac transthyretin amyloidosis: an observational report. *Clin. Res. Cardiol.* **2012**, *101*, 805−813.
(24) Ferreira, N.; Saraiva, M. J.; Almeida, M. R. Epigallocatechin-3-gallate as a potential therapeutic drug for TTR-related amyloidosis: "in vivo" evidence from FAP mice models. *PLoS ONE* **2012**, *7* (1), e29933.
(25) Clinical trials: safety and efficacy study of Fx-1006A in patients with familial amyloidosis. http://clinicaltrials.gov/ct2/show/NCT00409175. An extension of study Fx-005 evaluating long-term safety and clinical outcomes of Fx-1006A in patients with transthyretin amyloid polyneuropathy. http://clinicaltrials.gov/ct2/show/NCT00791492/.
(26) Coelho, T.; Maia, L. F.; Martins da Silva, A.; Waddington, Cruz, M.; Planté-Bordeneuve, V.; Lozeron, P.; Suhr, O. B.; Campistol, J. M.; Conceição, I. M.; Schmidt, H. H.; Trigo, P.; Kelly, J. W.; Labaudinière, R.; Chan, J.; Packman, J.; Wilson, A.; Grogan, D. R. Tafamidis for transthyretin familial amyloid polyneuropathy: a randomized, controlled trial. *Neurology* **2012**, *79*, 785−792.
(27) de Lartigue, J. Tafamidis for transthyretin amyloidosis. *Drugs Today* **2012**, *48*, 331−337.
(28) Bulawa, C. E.; Connelly, S.; Devit, M.; Wang, L.; Weigel, C.; Fleming, J. A.; Packman, J.; Powers, E. T.; Wiseman, R. L.; Foss, T. R.; Wilson, I. A.; Kelly, J. W.; Labaudinière, R. Tafamidis, a potent and selective transthyretin kinetic stabilizer that inhibits the amyloid cascade. *Proc. Natl. Acad. Sci. U.S.A.* **2012**, *109*, 9629−9634.
(29) Clinical trials: the effect of diflunisal on familial amyloidosis. http://clinicaltrials.gov/ct2/show/NCT00294671.
(30) Castaño, A.; Helmke, S.; Alvarez, J.; Delisle, S.; Maurer, M. S. Diflunisal for ATTR cardiac amyloidosis. *Congestive Heart Failure* **2012**, *18*, 315−319.
(31) Berk, J. L.; Suhr, O. B.; Sekijima, Y.; Yamashita, T.; Heneghan, M.; Zeldenrust, S. R.; Ando, Y.; Ikeda, S.; Gorevic, P.; Merlini, G.; Kelly, J. W.; Skinner, M.; Bisbee, A. B.; Dyck, P. J.; Obici, L. Familial amyloidosis consortium. The diflunisal trial: study accrual and drug tolerance. *Amyloid* **2012**, *19* (Suppl 1), 37−38.
(32) Obici, L.; Cortese, A.; Lozza, A.; Lucchetti, J.; Gobbi, M.; Palladini, G.; Perlini, S.; Saraiva, M. J.; Merlini, G. Doxycycline plus tauroursodeoxycholic acid for transthyretin amyloidosis: a phase II study. *Amyloid* **2012**, *19* (Suppl 1), 34−36.
(33) Cardoso, I.; Martins, D.; Ribeiro, T.; Merlini, G.; Saraiva, M. J. Synergy of combined doxycycline/TUDCA treatment in lowering Transthyretin deposition and associated biomarkers: studies in FAP mouse models. *J. Transl. Med.* **2010**, *8*, 74.
(34) Clinical trials: safety, efficacy and pharmacokinetics of doxycycline plus tauroursodeoxycholic acid in transthyretin amyloidosis. http://clinicaltrials.gov/ct2/show/NCT01171859/.
(35) Terazaki, H.; Ando, Y.; Fernandes, R.; Yamamura, K.; Maeda, S.; Saraiva, M. J. Immunization in familial amyloidotic polyneuropathy: counteracting deposition by immunization with a Y78F TTR mutant. *Lab. Invest.* **2006**, *86*, 23−31.
(36) Su, Y.; Jono, H.; Torikai, M.; Hosoi, A.; Soejima, K.; Guo, J.; Tasaki, M.; Misumi, Y.; Ueda, M.; Shinriki, S.; Shono, M.; Obayashi, K.; Nakashima, T.; Sugawara, K.; Ando, Y. Antibody therapy for familial amyloidotic polyneuropathy. *Amyloid* **2012**, *19* (Suppl 1), 45−46.
(37) Benson, M. D.; Pandey, S.; Witchell, D.; Jazayeri, A.; Siwkowski, A.; Monia, B.; Kluve-Beckerman, B. Antisense oligonucleotide therapy for TTR amyloidosis. *Amyloid* **2011**, *18* (Suppl 1), 60.
(38) Benson, M. D.; Kluve-Beckerman, B.; Zeldenrust, S. R.; Siesky, A. M.; Bodenmiller, D. M.; Showalter, A. D.; Sloop, K. W. Targeted suppression of an amyloidogenic transthyretin with antisense oligonucleotides. *Muscle Nerve* **2006**, *33*, 609−618.
(39) Nakamura, M.; Ando, Y. Applications of gene therapy for familial amyloidotic polyneuropathy. *Expert Opin. Biol. Ther.* **2004**, *4*, 1621−1627.
(40) Hamilton, J. A.; Benson, M. D. Transthyretin: a review from a structural perspective. *Cell. Mol. Life Sci.* **2001**, *58*, 1491−1521.
(41) Monaco, H. L.; Rizzi, M.; Coda, A. Structure of a complex of two plasma proteins: transthyretin and retinol-binding protein. *Science* **1995**, *268*, 1039−1041.

(42) Buxbaum, J. N.; Reixach, N. Transthyretin: the servant of many masters. *Cell. Mol. Life Sci.* **2009**, *66*, 3095−3101.
(43) Ingbar, S. H. Observations concerning the binding of thyroid hormones by human serum prealbumin. *J. Clin. Invest.* **1963**, *42*, 143−160.
(44) Blake, C. C. F.; Geisow, M. J.; Oatley, S. J.; Rérat, B.; Rérat, C. Structure of prealbumin: secondary, tertiary and quaternary interactions determined by Fourier refinement at 1.8 Å. *J. Mol. Biol.* **1978**, *121*, 339−356.
(45) Palaninathan, S. K. Nearly 200 X-ray crystal structures of transthyretin: what do they tell us about this protein and the design of drugs for TTR amyloidoses? *Curr. Med. Chem.* **2012**, *19*, 2324−2342.
(46) Berman, H. M; Westbrook, J.; Feng, Z.; Gilliland, G.; Bhat, T. N.; Weissig, H.; Shindyalov, I. N.; Bourne, P. E. The protein data bank. *Nucleic Acids Res.* **2000**, *28*, 235−242.
(47) Parisini, E.; Metrangolo, P.; Pilati, T.; Resnati, G.; Terraneo, G. Halogen bonding in halocarbon-protein complexes: a structural survey. *Chem. Soc. Rev.* **2011**, *40*, 2267−2678.
(48) Metrangolo, P.; Resnati, G. Chemistry. Halogen versus hydrogen. *Science* **2008**, *321*, 918−919.
(49) Metrangolo, P.; Neukirch, H.; Pilati, T.; Resnati, G. Halogen bonding based recognition processes: a world parallel to hydrogen bonding. *Acc. Chem. Res.* **2005**, *38*, 386−395.
(50) Politzer, P.; Murray, J. S. Halogen bonding: an interim discussion. *ChemPhysChem* **2013**, *14*, 278−294.
(51) Wilcken, R.; Zimmermann, M. O.; Lange, A.; Joerger, A. C.; Boeckler, F. M. Principles and applications of halogen bonding in medicinal chemistry and chemical biology. *J. Med. Chem.* **2013**, *56*, 1363−1388.
(52) Scholfield, M. R.; Zanden, C. M.; Carter, M.; Ho, P. S. Halogen bonding (X-bonding): a biological perspective. *Protein Sci.* **2013**, *22*, 139−152.
(53) Hardegger, L. A.; Kuhn, B.; Spinnler, B.; aAnselm, L.; Ecabert, R.; Stihle, M.; Gsell, B.; Thoma, R.; Diez, J.; Benz, J.; Plancher, J. M.; Hartmann, G.; Banne, D. W.; Haap, W.; Diederich, F. Systematic investigation of halogen bonding in protein−ligand interactions. *Angew. Chem., Int. Ed.* **2011**, *50*, 314−318.
(54) Lu, Y.; Liu, Y.; Xu, Z.; Li, H.; Liu, H.; Zhu, W. Halogen bonding for rational drug design and new drug discovery. *Expert Opin. Drug Discov.* **2012**, *7*, 375−383.
(55) Lu, Y.; Shi, T.; Wang, Y.; Yang, H.; Yan, X.; Luo, X.; Jiang, H.; Zhu, W. Halogen bonding—a novel interaction for rational drug design? *J. Med. Chem.* **2009**, *52*, 2854−2862.
(56) Gales, L.; Macedo-Ribeiro, S.; Arsequell, G.; Valencia, G.; Saraiva, M. J.; Damas, A. M. Human transthyretin in complex with iododiflunisal: structural features associated with a potent amyloid inhibitor. *Biochem. J.* **2005**, *388*, 615−621.
(57) Dolado, I.; Nieto, J.; Saraiva, M. J.; Arsequell, G.; Valencia, G.; Planas, A. Kinetic assay for high-throughput screening of in vitro transthyretin amyloid fibrillogenesis inhibitors. *J. Comb. Chem.* **2005**, *7*, 246−252.
(58) Arsequell, G.; Planas, A. Methods to evaluate the inhibition of TTR fibrillogenesis induced by small ligands. *Curr. Med. Chem.* **2012**, *19*, 2343−55.
(59) Desiraju, G. R.; Ho, P. S.; Kloo, L.; Legon, A. C.; Marquardt, R.; Metrangolo, P.; Politzer, P.; Resnati, G.; Rissanen, K. Definition of the halogen bond (IUPAC Recommendations 2013)*. *Pure Appl. Chem.* **2013**, *85*, 1711−1713.
(60) Auffinger, P.; Hays, F. A.; Westhof, E.; Ho, P. S. Halogen bonds in biological molecules. *Proc. Natl. Acad. Sci. U.S.A.* **2004**, *101*, 16789−16794.
(61) Wilcken, R.; Liu, X.; Zimmermann, M. O.; Rutherford, T. J.; Fersht, A. R.; Joerger, A. C.; Boeckler, F. M. Halogen-enriched fragment libraries as leads for drug rescue of mutant p53. *J. Am. Chem. Soc.* **2012**, *134*, 6810−6818.
(62) Fanfrlik, J.; Kolář, M.; Kamlar, M.; Hurny, D.; Ruiz, F. X.; Cousido-Siah, A.; Mitschler, A.; Rezáč, J.; Munusamy, E.; Lepsik, M.; Matejicek, P.; Vesely, J.; Podjarny, A. Hobza, P. The modulation of aldose reductase inhibition by halogen bond tuning. *ACS Chem. Biol.* **2013** [Online early access]. DOI: 10.1021/cb400526n. Published Online: August 30, 2013.
(63) Bent, H. A. Structural chemistry of donor−acceptor interactions. *Chem. Rev.* **1968**, *68*, 587−648.
(64) Hassel, O. Structural aspects of interatomic charge−transfer bonding. *Science* **1970**, *170*, 497−502.
(65) Gales, L.; Almeida, M. R.; Arsequell, G.; Valencia, G.; Saraiva, M. J.; Damas, A. M. Iodination of salicylic acid improves its binding to transthyretin. *Biochem. Biophys. Acta* **2008**, *1784*, 512−517.
(66) Choi, S.; Reixach, N.; Connelly, S.; Johnson, S. M.; Wilson, I. A.; Kelly, J. W. A substructure combination strategy to create potent and selective transthyretin kinetic stabilizers that prevent amyloidogenesis and cytotoxicity. *J. Am. Chem. Soc.* **2010**, *132*, 1359−1370.
(67) Eneqvist, T.; Lundberg, E.; Karlson, A.; Huang, S.; Santos, C. R.; Power, D. M.; Sauer-Eriksson, A. E. High resolution crystal structures of piscine transthyretin reveal different binding modes for triiodothyronine and thyroxine. *J. Biol. Chem.* **2004**, *279*, 26411−26416.
(68) Adamski-Werner, S. L.; Palaninathan, S. K; Sacchettini, J. C.; Kelly, J. W. Diflunisal analogues stabilize the native state of transthyretin. Potent inhibition of amyloidogenesis. *J. Med. Chem.* **2004**, *47*, 355−374.
(69) Baures, P. W.; Oza, V. B.; Peterson, S. A.; Kelly, J. W. Synthesis and evaluation of inhibitors of transthyretin amyloid formation based on the non-steroidal anti-inflammatory drug, flufenamic acid. *Bioorg. Med. Chem.* **1999**, *7*, 1339−1347.
(70) Mairal, T.; Nieto, J.; Pinto, M.; Almeida, M. R.; Gales, L.; Ballesteros, A.; Barluenga, J.; Pérez, J. J.; Vázquez, J. T; Centeno, N. B.; Saraiva, M. J.; Damas, A. M.; Planas, A.; Arsequell, G.; Valencia, G. Iodine atoms: a new molecular feature for the design of potent transthyretin fibrillogenesis inhibitors. *PLoS ONE* **2009**, *4* (1), e4124.
(71) Goodford, P. J. A computational procedure for determining energetic favourable binding site of biological important macromolecules. *J. Med. Chem.* **1985**, *28*, 849−857.
(72) Neumann, P.; Cody, V.; Wojtczak, A. Structural basis of negative cooperativity in transthyretin. *Acta Biochim. Pol.* **2001**, *48*, 867−875.
(73) Trivella, D. B.; Sairre, M. I.; Foguel, D.; Lima, L. M.; Polikarpov, I. The binding of synthetic triiodo L-thyronine analogs to human transthyretin: molecular basis of cooperative and non-cooperative ligand recognition. *J. Struct. Biol.* **2011**, *173*, 323−332.
(74) Almeida, M. R.; Macedo, B.; Cardoso, I.; Alves, I.; Valencia, G.; Arsequell, G.; Planas, A.; Saraiva, M. J. Selective binding to transthyretin and tetramer stabilization in serum from patients with familial amyloidotic polyneuropathy by an iodinated diflunisal derivative. *Biochem. J.* **2004**, *381*, 351−356.
(75) Blasi, D.; Pinto, M.; Nieto, J.; Arsequell, G.; Valencia, G.; Planas, A.; Centeno, N. B.; Quintana, J. Drug discovery targeted at transthyretin cardiac amyloidosis: rational design, synthesis, and biological activity of new transthyretin amyloid inhibitors. *Amyloid* **2011**, *18* (Suppl 1), 55−57.
(76) Pinto, M.; Blasi, D.; Nieto, J.; Arsequell, G.; Valencia, G.; Planas, A.; Quintana, J.; Centeno, N. B. Ligand-binding properties of human transthyretin. *Amyloid* **2011**, *18* (Suppl 1), 51−54.
(77) Bondi, A. van der Waals volumes and Radii. *J. Phys. Chem.* **1964**, *68*, 441−451.
(78) Wilcken, R.; Zimmermann, M. O.; Lange, A.; Zahn, S.; Boeckler, F. M. Using halogen bonds to address the protein backbone: a systematic evaluation. *J. Comput. Aided Mol. Des.* **2012**, *26*, 935−945.
(79) Peterson, S. A.; Klabunde, T.; Lashuel, H. A.; Purkey, H.; Sacchettini, J. C.; Kelly, J. W. Inhibiting transthyretin conformational changes that lead to amyloid fibril formation. *Proc. Natl. Acad. Sci. U. S. A.* **1998**, *95*, 12956−12960.
(80) Purkey, H. E.; Palaninathan, S. K.; Kent, K. C.; Smith, C.; Safe, S. H.; Sacchettini, J. C.; Kelly, J. W. Hydroxylated polychlorinated biphenyls selectively bind transthyretin in blood and inhibit amyloidogenesis: rationalizing rodent PCB toxicity. *Chem. Biol.* **2004**, *11*, 1719−1728.
(81) Zanotti, G.; D'Acunto, M. R.; Malpeli, G.; Folli, C.; Berni, R. Crystal structure of the transthyretin−retinoic−acid complex. *Eur. J. Biochem.* **1995**, *234*, 563−569.

(82) Morais-de-Sá, E.; Neto-Silva, R. M.; Pereira, P. J.; Saraiva, M. J.; Damas, A. M. The binding of 2,4-dinitrophenol to wild-type and amyloidogenic transthyretin. *Acta Crystallogr., Sect. D: Biol. Crystallogr.* **2006**, *62*, 512−519.
(83) Wojtczak, A.; Cody, V.; Luft, J. R.; Pangborn, W. Structures of human transthyretin complexed with thyroxine at 2.0 Å resolution and 3′,5′-dinitro-*N*-acetyl-L-thyronine at 2.2 Å resolution. *Acta Crystallogr., Sect. D: Biol. Crystallogr.* **1996**, *52*, 758−765.
(84) Neumann, P.; Cody, V.; Wojtczak, A. Ligand binding at the transthyretin dimer-dimer interface: structure of the transthyretin−T4Ac complex at 2.2 Angstrom resolution. *Acta Crystallogr., Sect. D: Biol. Crystallogr.* **2005**, *61*, 1313−1319.
(85) Morais-de-Sá, E.; Pereira, P. J.; Saraiva, M. J.; Damas, A. M. The crystal structure of transthyretin in complex with diethylstilbestrol: a promising template for the design of amyloid inhibitors. *J. Biol. Chem.* **2004**, *279*, 53483−53490.
(86) Wade, R. C.; Clark, K. J.; Goodford, P. J. Further development of hydrogen bond functions for use in determining energetically favorable binding sites on molecules of known structure. 1. Ligand probe groups with the ability to form two hydrogen bonds. *J. Med. Chem.* **1993**, *36*, 140−147.
(87) Wade, R. C.; Goodford, P. J. Further development of hydrogen bond functions for use in determining energetically favorable binding sites on molecules of known structure. 2. Ligand probe groups with the ability to form more than two hydrogen bonds. *J. Med. Chem.* **1993**, *36*, 148−156.
(88) Pastor, M.; Cruciani, G.; Watson, K. A. A strategy for the incorporation of water molecules present in a ligand binding site into a three-dimensional quantitative structure-activity relationship analysis. *J. Med. Chem.* **1997**, *40*, 4089−4102.
(89) Cornell, W.; Cieplak, P.; Bayley, C. I.; Gould, I.; Merz, K. M.; Ferguson, D. M.; Spellmeyer, D. C.; Fox, T.; Caldwell, J. W.; Kollman, P. A. A Second Generation Force Field for the Simulation of Proteins, Nucleic Acids, and Organic Molecules. *J. Am. Chem. Soc.* **1995**, *117*, 5179−5197.
(90) Case, D. A.; Pearlman, D. A.; Caldwell, J. W.; Cheatham III, T. E.; Ross, W. S.; Simmerling, C. L.; Darden, T. A.; Merz, K. M.; Stanton, R. V.; Cheng, A. L.; Vincent, J. J.; Crowley, M.; Tsui, V.; Radmer, R. J.; Duan, Y.; Pitera, J.; Massova, I.; Seibel, G. L.; Singh, U. C.; Weiner, P. K.; Kollman, P. A. AMBER 6; University of California: San Francisco, CA, 1999.
(91) Frisch, M. J.; Trucks, G. W.; Schlegel, H. B.; Gill, P. M. W.; Johnson, B. G.; Robb, M. A.; Cheeseman, J. R.; Keith, T.; Petersson, G.; Montgomery, J. A.; Raghavachari, K.; Al-Laham, M. A.; Zakrzewski, V. G.; Ortiz, J. V.; Foresman, J. B.; Cioslowski, J.; Stefanov, B. B.; Nanayakkara, A.; Challacombe, M.; Peng, C. Y.; Ayala, P. Y.; Chen, W.; Wong, M. W.; Andres, J. L.; Replogle, E. S.; Gomperts, R.; Martin, R. L.; Fox, D. J.; Binkley, J. S.; Defrees, D. J.; Baker, J.; Stewart, J. P.; Head-Gordon, M.; Gonzalez, C.; Pople, J. A. *Gaussian 94*, revision E.1; Gaussian, Inc.: Pittsburgh, PA, 1996.
(92) Bayly, C. I.; Cieplak, P.; Cornell, W.; Kollman, P. A. A well-behaved electrostatic potential based method using charge restraints for deriving atomic charges: the RESP model. *J. Phys. Chem.* **1993**, *97*, 10269−10280.